

# We are IntechOpen, the world's leading publisher of Open Access books Built by scientists, for scientists

6,900

Open access books available

185,000

International authors and editors

200M

Downloads

Our authors are among the

154

Countries delivered to

TOP 1%

most cited scientists

12.2%

Contributors from top 500 universities



WEB OF SCIENCE™

Selection of our books indexed in the Book Citation Index  
in Web of Science™ Core Collection (BKCI)

Interested in publishing with us?  
Contact [book.department@intechopen.com](mailto:book.department@intechopen.com)

Numbers displayed above are based on latest data collected.  
For more information visit [www.intechopen.com](http://www.intechopen.com)



# Amorphous and Crystalline Silicon Films from Soluble Si-Si Network Polymers

Michiya Fujiki<sup>1</sup> and Giseop Kwak<sup>2</sup>

<sup>1</sup>Graduate School of Materials Science, Nara Institute of Science and Technology

<sup>2</sup>Department of Polymer Science, Kyungpook National University

<sup>1</sup>Japan

<sup>2</sup>Korea

## 1. Introduction

Silicon (Si) is the second most abundant element (Clarke number ~26%) on Earth and exists mainly in the oxidized silicate (SiO<sub>2</sub>) form. Si sources are neither localized in very specific regions nor are they noble. However, crystalline (*c*-Si) and amorphous (*a*-Si) silicons remain the most fundamental, purely inorganic materials used for microelectronics, optoelectronics, and photonics because the lithographic and *p-n* doping processes are already well-established in industry. To produce these materials, vacuum and vapor-phase deposition processes and mechanical slicing/polishing techniques of Si-wafers are invariably utilized. However, these techniques require the use of an expensive XeCl excimer laser for annealing of *a*-Si; this step is followed by a crystallization process to prepare a poly-Si thin film transistor (TFT) from a *a*-Si thin film, which is deposited using a highly dangerous SiH<sub>4</sub>-Si<sub>2</sub>H<sub>6</sub> chemical vapor deposition (CVD) process.

### 1.1 Physical and chemical approaches for controlling the band gap of crystalline silicon

There are many types of Si-based materials ranging from zero-dimensional (0D) nanocrystalline silicon (*nc*-Si) and nanoparticles, one-dimensional (1D) polysilane and nanowire, and two-dimensional (2D) Si-skeletons, including Si-Si bonded network polysilyne (SNP), Wöhler siloxene, and Si/SiO<sub>2</sub> superlattice, to three-dimensional (3D) Si-skeletons, including *c*-Si and *a*-Si (Table 1).

The fundamental materials for microelectronics, *c*-Si and *a*-Si, are poor UV-visible-near IR emitters with low quantum yields ( $\Phi_F$ ) of ~10<sup>-2</sup>% at 300 K because of their narrow band gap (1127 nm, 1.1 eV) with indirect electronic transitions (Lockwood, 1998; Yu & Cardona, 2005). Since the first reports of fairly efficient photoluminescence (PL) in the visible-near IR region from *nc*-Si (Furukawa & Miyasato, 1988; Takagi et al., 1990; Kanemitsu et al., 1993; Kanemitsu et al., 1995; Kanemitsu et al., 1996; Wilson et al., 1993) and porous Si (Cullis & Canham, 1991; Cullis et al., 1997; Lehmann & Gösele, 1991; Heitmann et al., 2005), extensive research efforts have been expended to produce Si with efficient, tunable UV-visible emission. To effectively confine a photoexcited electron-hole pair (exciton) within Si's Bohr radius ( $r_B$ ) of ~5 nm (Lockwood, 1998; Yu & Cardona, 2005), various low-dimensional Si-based materials have been theoretically (Takeda & Shiraishi, 1997; Takeda & Shiraishi, 1998;

Brus, 1994; Alivisatos, 1996) and experimentally explored as follows: (a) 0D and 1D materials as visible-near IR emitters, including *nc*-Si and nanoparticles (Holmes et al., 2001; Grom et al., 2000; Kovalev et al., 1998; Gelloz et al., 2005; Walters et al., 2006; Jurbergs et al., 2006; English et al., 2002; Fojtik & Henglein, 1994; Li et al., 2004; Liu et al., 2005; Choi et al., 2007; Watanabe, 2003; Pi et al., 2008; Liu, 2008; Bley & Kauzlarich, 1996; Mayeri et al., 2001; Zou et al., 2004; Zhang et al., 2007; Wilcoxon et al., 1999; Hua et al., 2006; Nayfeh & Mitas, 2008) and Si nanowires (Qi et al., 2003; Ma et al., 2005); (b) 1D materials as excitonic UV emitters, including chain-like polysilane (Fujiki, 2001; Hasegawa et al., 1996); (c) 2D Si skeletons as visible emitters, including Si-Si bonded network polymers (SNP) (Takeda & Shiraishi, 1997; Bianconi et al., 1989; Bianconi & Weidman, 1988; Furukawa et al., 1990; Wilson & Weidman, 1991), Wöhler siloxenes (Brandt et al., 2003), and a Si/SiO<sub>2</sub> superlattice (Lu et al., 1995). Although SNPs have been regarded as soluble precursor polymers of *a*-Si (Wilson & Weidman, 1991) and 2D-Si nanosheets (saturated, bonded "sila-graphene") (Brandt et al., 2003; Nesper, 2003), further studies on the pyrolytic products of SNP derivatives and their inherent photophysical properties in a vacuum at low temperature have not yet been reported.

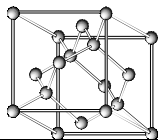
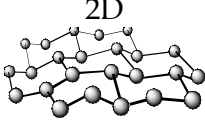
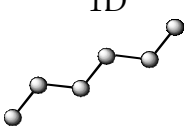
4A- elements	Dimensionality and $E_g$ (eV) (Brus, 1994; Takeda & Shiraishi, 1989)		
	 3D	 2D	 1D
C	5.5 (IG)	-	~8
Si	1.1 (IG)	2.3 (IG and DG)	~4 (DG)
Ge	0.7 (IG)	1.8 (IG and DG)	~4 (DG)
Sn	0.1	-	~ 3 (DG)
Pb	~0	-	-

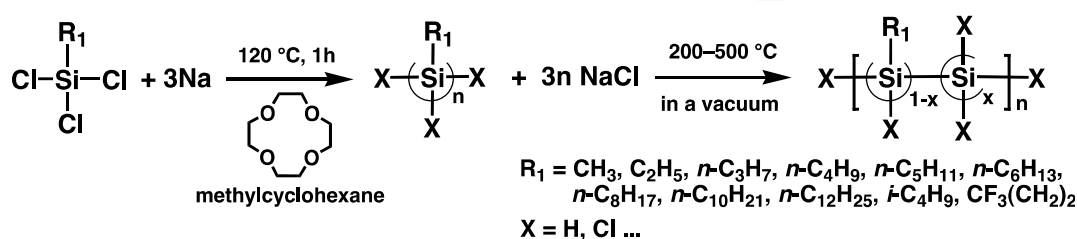
Table 1. Schematic concept of skeleton dimensionality and elements. *DG*: Direct gap, *IG*: Indirect gap.

Solution processing of metal chalcogenide semiconductors to fabricate stable and high-performance transistors has recently been developed (Alivisatos, 1996). To produce *c*-Si, *a*-Si, and new Si-based materials with controlled optical band gaps, low-cost solution and thermal production methods that are environmentally friendly and safe and can deposit Si on a plastic film at lower temperatures (below 250 °C) using soluble Si-source materials are greatly preferable. Among the Si source materials, organosilicon compounds may be some of the most promising candidates to satisfy the above criteria in actual Si-device fabrication processes because organosilicon compounds are usually air-stable, non-toxic, non-flammable, non-explosive, and soluble in common organic solvents. Through re-evaluation of previously reported research, we endeavor to advance our knowledge and understanding of Si-related materials science. Among the Si-related materials mentioned above, SNPs are especially interesting as soluble precursor polymers to pyrolytically transform into 3D Si-skeleton materials. In this chapter, we establish strong evidence that SNP is one of the most promising, air-stable, soluble Si-source materials for the straightforward production of *c*-Si, *a*-Si, and controlled bang-gap Si-based materials via simple control of the organic side groups of SNP as well as the

vacuum pyrolysis conditions, including the pyrolysis temperature, pyrolysis time, and the presence of a trace amount of air.

## 1.2 Soluble silicon network polymers bearing organic groups

Various SNPs can be prepared via a one-step condensation reaction of the corresponding, non-flammable, non-toxic alkyltrichlorosilanes with sodium in 50–60% yield at 120 °C in inert organic solvent. A liquid NaK alloy and ultrasonic wave (USW) irradiation were applied in the preparation of the first SNP (Bianconi et al., 1989; Bianconi and Weidman, 1988). Subsequently, the use of Na metal with catalytic amounts of crown ethers readily afforded these SNPs in milder and safer conditions without USW irradiation, as shown in Scheme 1 (Furukawa et al., 1990).



Scheme 1. General synthesis and vacuum-pyrolysis procedures for the preparation of SNPs.

In the present study, SNPs were prepared by the modified Na-mediated reduction (Wurtz-Kipping reaction) of the corresponding alkyltrichlorosilanes in the presence of 12-crown-4-ether as co-catalyst under a N<sub>2</sub> atmosphere (Fujiki et al., 2009). The SNPs were protected from contact with air and moisture during all of the synthetic procedures, including preparation, isolation, and sample enclosure in a glass tube. The SNPs were typically synthesized as shown in Scheme 1. For example, methylcyclohexane (4 mL, dried over 4 Å molecular sieves) containing Na (0.43 g, 19 mmol) and 12-crown-4-ether (0.02 g, 0.11 mmol) was placed in a four-necked 100 mL flask and refluxed at the relatively high temperature of 120 °C with vigorous mechanical stirring. To this mixture, *n*-butyltrichlorosilane (0.98 g, 5.1 mmol) dissolved in methylcyclohexane (4 mL) was added drop-wise. After the addition was complete, the solution was stirred for 1 h and then allowed to cool to room temperature. The reaction vessel was transferred to a glove box filled with 99.9% N<sub>2</sub> gas. To remove excess Na and NaCl, the reaction mixture was filtered using a fluorinated membrane filter (0.50 μm pore size) under pressure to yield a clear yellow solution containing *n*-butyl-substituted SNP (*n*-BSNP). The polymer was isolated by precipitating the solution in dry acetone and then dried in the glove box via connection to an external vacuum pump. Ethyl, *n*-propyl, *i*-butyl, *n*-pentyl, *n*-hexyl, *n*-octyl, *n*-decyl, *n*-dodecyl, and 3,3,3-trifluoropropyl-substituted SNP derivatives were similarly prepared as soluble polymers. Only methyl-substituted SNP was insoluble in all solvents, due to its very short alkyl group. The yields of SNPs ranged from 40–50%. Weight-averaged and number-averaged molecular weights (*M<sub>w</sub>* and *M<sub>n</sub>*) of the soluble SNPs ranged from 3–43 × 10<sup>3</sup> g mol<sup>-1</sup>. Freshly-prepared SNPs did not exhibit any IR absorption due to the Si-O-Si stretching vibration of the oxidized Si-Si bond around 1000–1100 cm<sup>-1</sup>.

A methylcyclohexane solution of SNPs was transferred into glass tubes (ID 5 mm, OD 7 mm); the inner wall of the tube was manually coated with the solution, and the solution was dried by blowing with N<sub>2</sub> gas. The SNP films deposited in the glass tubes were connected to a two-way vacuum bulb. The glass tubes coated with the SNP films were removed from the

glove box and sealed using a hand-burner using vacuum techniques (0.3 Torr by rotary pump or  $5 \times 10^{-5}$  Torr by a Pfeiffer turbo molecular pump). For pyrolysis experiments and photoluminescence (PL)/PL excitation (PLE) measurements, the glass tubes were placed into a housing made of an aluminum block and then onto a digitally-controlled hotplate (Thermolyne), and the temperature of the housing was monitored with a chromel-alumel thermocouple.

### 1.3 Pyrolysis of Si-containing polymers

Pyrolysis of several Si-containing polymers, including poly(dimethylsilane) (Yajima et al., 1978), polycarbosilane (PCS) (Liu et al., 1999; Schmidt et al., 1991), and polysilane-containing chlorine (Martin et al., 1997), is well-known to produce  $\beta$ -silicon carbide exclusively ( $\beta$ -SiC). This fact engendered the idea that SNPs might also produce  $\beta$ -SiC as a result of pyrolysis. However, thermogravimetric (TG) and isothermal thermogravimetric (ITG) analyses of ten SNPs in a stream of pure nitrogen gas indicated that elemental Si was produced.

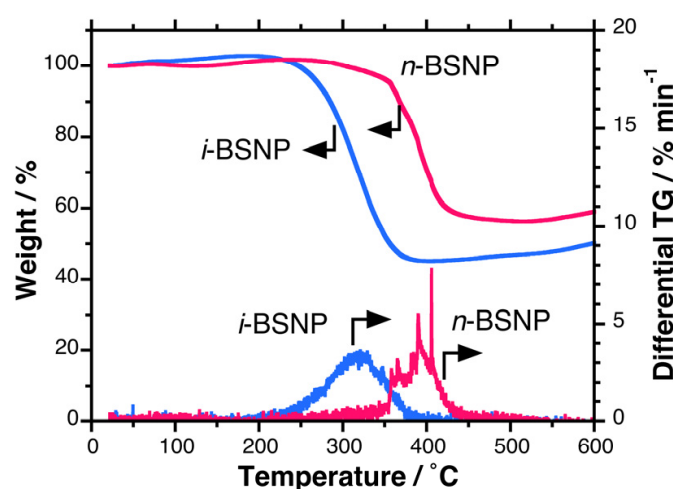
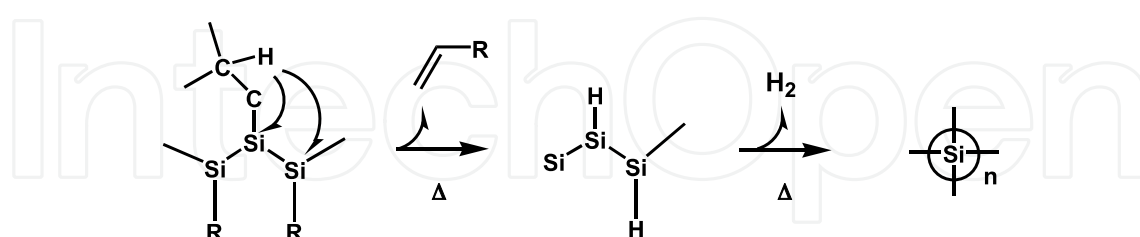


Fig. 1. Thermogravimetric (TG) and differential thermogravimetric (DTG) analysis curves of *n*-BSNP and *i*-BSNP in a N<sub>2</sub> atmosphere (heating rate = 5 °C min<sup>-1</sup>).



Scheme 2. Proposed mechanism of the  $\beta$ -H shift from the alkyl group to the Si-Si bonded skeleton.

The TG analysis data showed that SNPs undergo degradation in two steps (Fig. 1). With the exception of sterically-overcrowded isobutyl- and trifluoropropyl-substituted SNP derivatives (*i*-BSNP and FPSNP), most SNPs began to degrade at  $\sim 300$  °C (not shown here), suggesting that an alkylene moiety is eliminated due to a  $\beta$ -H shift from the alkyl group to the Si skeleton, followed by the release of H<sub>2</sub> gas from the Si-H bond at  $\sim 450$  °C. In contrast, the *i*-BSNP and FPSNP derivatives began to degrade at temperatures as low as

~250 °C. The proposed SNP pyrolysis mechanism is shown in Scheme 2. ITG data for SNPs at 500 °C as a function of pyrolysis time (Fig. 2) suggests that the observed weight loss of the SNP after prolonged (90 min) pyrolysis corresponds to a residue of pure Si (*not* SiC), regardless of alkyl side group (Fig. 3). This result was further confirmed by scanning electron microscopy (SEM)/X-ray photoelectron spectroscopy (XPS)/energy dispersive X-ray spectroscopy (EDS) analyses of the product yielded by pyrolysis of *n*-propyl-SNP and *n*-butyl-SNP (*n*-BSNP) at 900 °C, which showed that the surface was oxidized, as evidenced by 1:1 signals of Si and O but no detectable C signal due to SiC (Fig. 4 and Fig. 5).

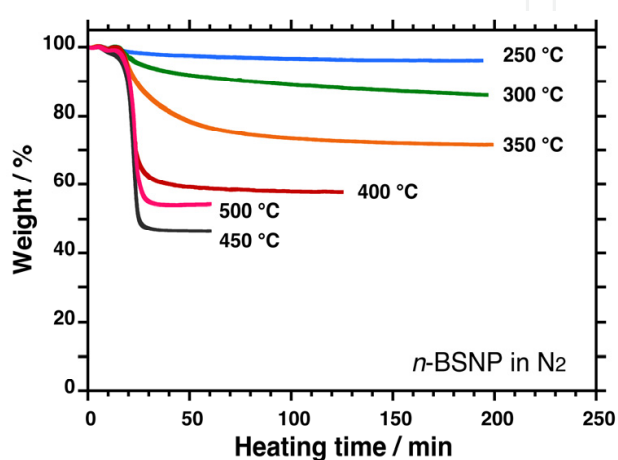


Fig. 2. Isothermal thermogravimetric (ITG) analysis curves of *n*-BSNP in a stream of N<sub>2</sub> gas at selected temperatures. ITG curves between 450 °C and 500 °C appeared to be reversed. This result was reproducible, probably due to rapid evolution of some volatile products from *n*-BSNP during prolonged heating at 450 °C.

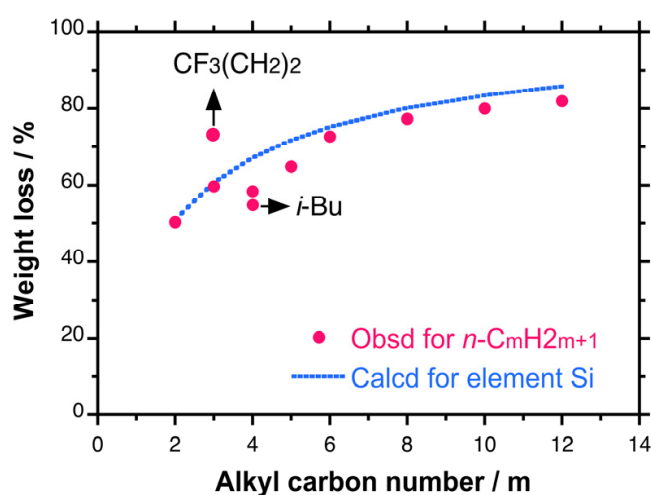


Fig. 3. Weight loss values of ten SNPs bearing different alkyl side chains upon pyrolysis at 500 °C for 90 min. Filled circles and dotted lines are experimental and calculated weight values for elemental Si, respectively.



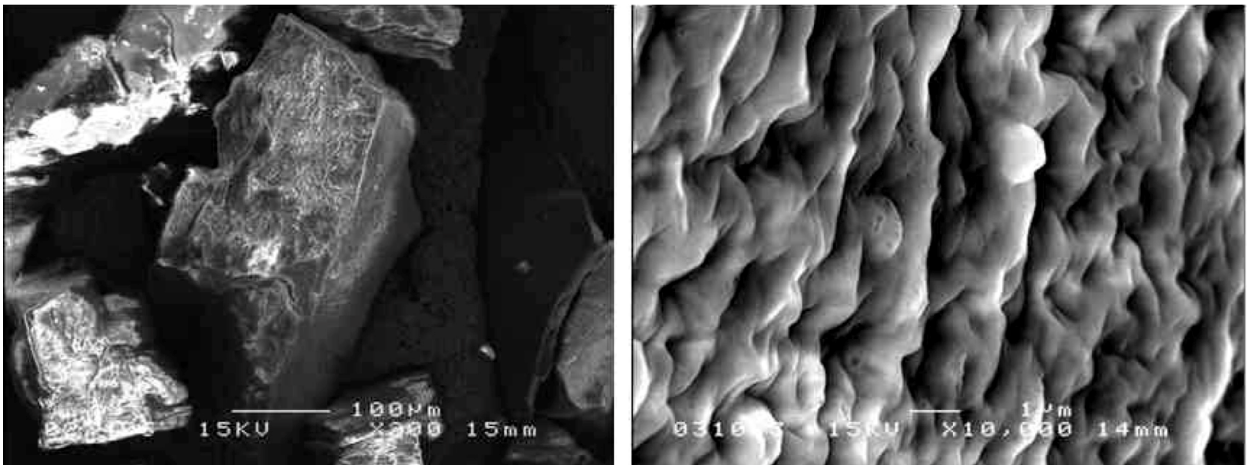


Fig. 4. Scanning electron microscope (SEM) images of *n*-propyl SNP pyrolyzed at 900 °C in a N<sub>2</sub> atmosphere (scale bars: left, 100 μm, and right, 1 μm).

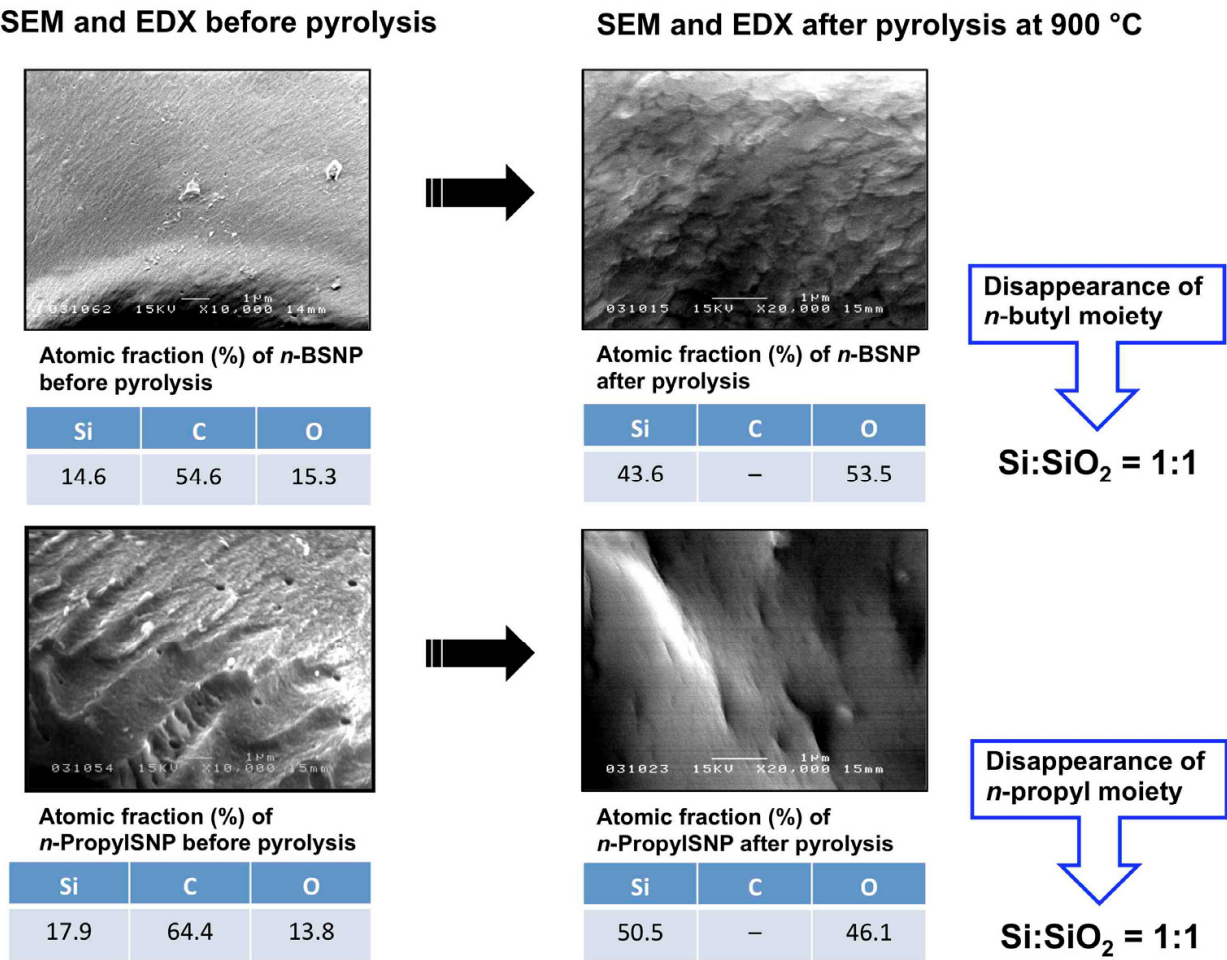
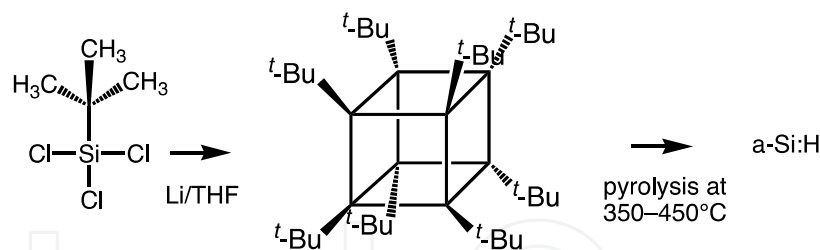
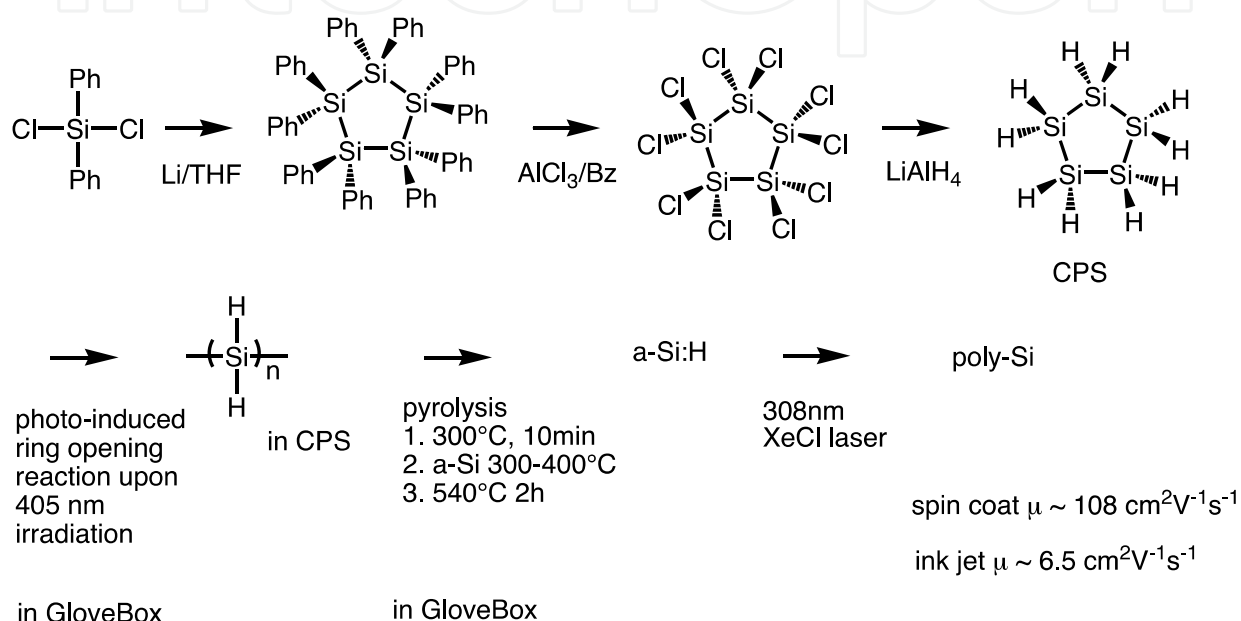


Fig. 5. Surface analysis of *n*-BSNP and *n*-propyl SNP by SEM and energy dispersive X-ray spectroscopy (EDS) before and after pyrolysis at 900 °C.



Scheme 3. The pyrolysis of octa(*tert*-butyl)octasilacubane (Furukawa, 2000).



Scheme 4. The pyrolysis of hydrogenated polysilane prepared via a four-step synthesis from diphenyldichlorosilane as a starting material (Shimoda et al., 2006).

Based on pyrolysis experiments with PCS (Liu et al., 1999; Schmidt et al., 1991),  $\beta$ -H elimination from alkyl C-H (Scheme 2) is postulated to be the key for producing elemental Si without significant interference by the Kumada rearrangement reaction responsible for  $\beta$ -SiC production (Shini and Kumada, 1958). Peripheral SNP structures may be terminated with Si-Cl and Si-H, as exemplified in chlorine-containing polysilane (Martin et al., 1997). For most SNPs, the existence of Si-Cl and Si-H bonds were evidenced by  $^{29}\text{Si}$ -NMR signals at  $\sim 30$  ppm and from the FT-IR signal around  $2080 \text{ cm}^{-1}$ , respectively (Fujiki et al., 2009). The free Cl atom from the Si-Cl bond may catalyze efficient  $\beta$ -H elimination. This unexpected result may be a common feature of reactions involving Si-Si bonded molecules and polymers bearing appropriate side groups in an oxygen-free environment. Indeed, an Si-Si bonded cubic molecule with bulky organic groups, *tert*-butyl-containing octasilacubane was transformed into an *a*-Si film via pyrolysis in a vacuum at  $350\text{--}450^\circ\text{C}$  (Scheme 3) (Furukawa, 2000). A polycrystalline Si thin film with a high-carrier mobility was prepared via pyrolysis of a Si-Si bonded linear polymer,  $(\text{SiH}_2)_n$ , at  $300\text{--}550^\circ\text{C}$  in an oxygen-free glove box (Shimoda et al., 2006). This hydrogenated polysilane was produced by a four-step synthesis, including a photo-induced ring-opening process, using diphenyldichlorosilane as a starting material (Scheme 4).



## 2. A new family of silicon network polymers as a precursor for c-Si, a-Si, and other Si-based materials

### 2.1 Controlled vacuum pyrolysis with a trace amount of air

TGA and ITGA data for the ten SNPs in pure N<sub>2</sub> gas (99.99%) indicated that elemental Si was produced. To confirm this result, laser Raman scattering spectra and microscope imaging of the *n*-BSNP pyrolyzed at 500 °C for 10 and 90 min were compared with the freshly-prepared *n*-BSNP film (Fig. 6). Several particles with a size of ~30 μm were observed in the *n*-BSNP pyrolyzed at 500 °C for 90 min. The regions with a metallic luster showed a sharp Raman resonance at 508 cm<sup>-1</sup> due to *nc*-like-Si particles, whereas regions with a non-metallic luster (amorphous regions) showed a very broad Raman shift at ~480 cm<sup>-1</sup>, similar to the freshly-prepared *n*-BSNP film.

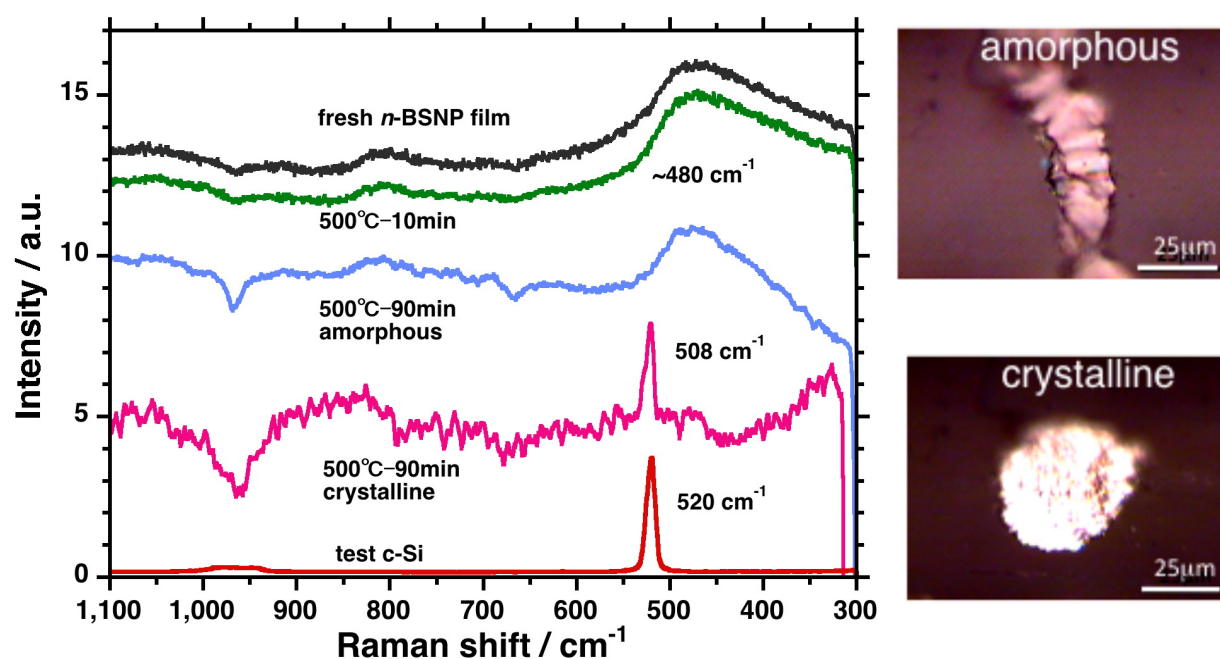


Fig. 6. Laser Raman scattering spectra and optical microscopy images of *n*-BSNP pyrolyzed at 500 °C.

### 2.2 Photophysical properties: photoluminescence and absorption spectra

The photoluminescence (PL) emission spectra of the ten soluble SNPs (Scheme 1) were measured between 460 nm and 740 nm (2.70-1.68 eV) at 77 K and at room temperature with controlled pyrolysis temperature (200~500 °C) and time (10~90 min) in a vacuum. The changes in the PL spectra of *n*-BSNP and *i*-BSNP films excited at 360 nm and 77 K, treated at several different pyrolysis temperatures for 10 and 90 min, are summarized in Fig. 7 (bottom) along with several color photographs of these *n*-BSNP films (Fig. 7, top).

Before pyrolysis, the freshly-prepared *n*-BSNP film emitted a yellowish PL, corresponding to a band maximum at 560 nm, with two fast lifetime components of 1.3 and 5.8 nsec. When the film was treated at 250 °C for 90 min, the PL band was markedly blue-shifted, exhibiting a blue PL band at 460 nm.

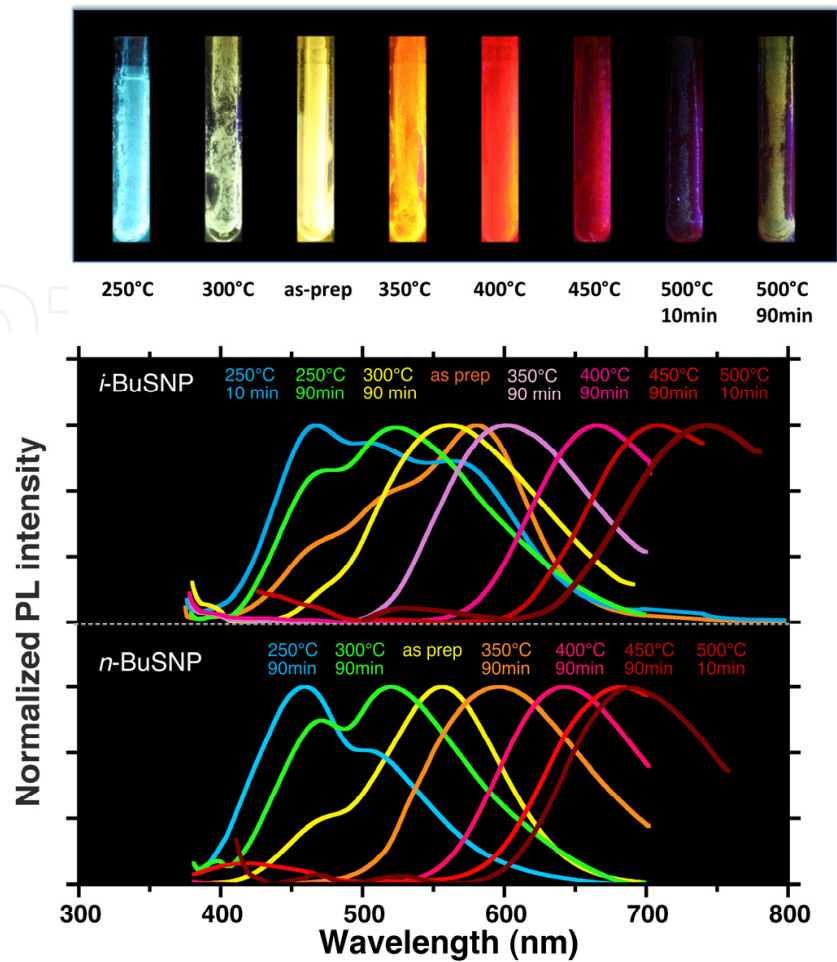


Fig. 7. Emission color photographs (top) and PL spectra (bottom) of *n*-BSNP and *i*-BSNP films pyrolyzed at different pyrolysis temperatures for different time periods (excited at 360 nm at 77 K).

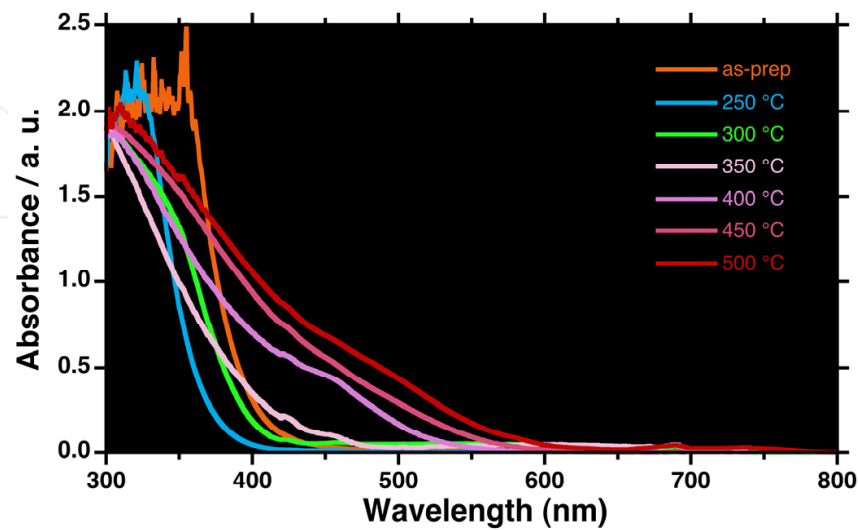


Fig. 8. UV-visible absorption spectra (normalized at 300 nm) of *n*-BSNP films pyrolyzed at different temperatures.

When the virgin films were treated at 300 °C for 90 min, the PL band was shifted slightly to green, corresponding to a peak maximum at 520 nm. Conversely, when the freshly-prepared films were treated at 350 °C, 400 °C, and 450 °C for 90 min, the PL wavelength was progressively red-shifted to orange at 580 nm, to red at 640 nm, and to deep-red at 680 nm. Similarly, the *i*-BSNP film progressively shifted first towards the blue region and then towards the red region. When the freshly-prepared *i*-BSNP film was treated at 500 °C for 10 min, the deepest red PL, corresponding to a peak maximum at 740 nm, was observed. Both *n*-BSNP or *i*-BSNP treated at 250–300 °C for 90 min exhibited a greenish-white emission to the naked eye.

When the freshly-prepared *n*-BSNP film was extensively heated at 500 °C for 90 min, it became a lustrous, metallic film that emitted a very weak, deep-red PL at approximately 680 nm with a marked decrease in intensity that was one-sixth that of the sample treated at 500 °C for 10 min. Figure 8 shows these marked, progressive blue- and red-shifts in the UV-visible absorption edge of pyrolyzed *n*-BSNP films maintained in sealed tubes at increasing pyrolysis temperatures. This change in the UV-visible absorption edge corresponds well to the blue- and red-shifts of the PL bands. It is noteworthy that the SNP film treated at 500 °C clearly showed broad absorption bands in the range of 350–600 nm, indicating that a significant change occurred in the Si-Si bonded skeleton.

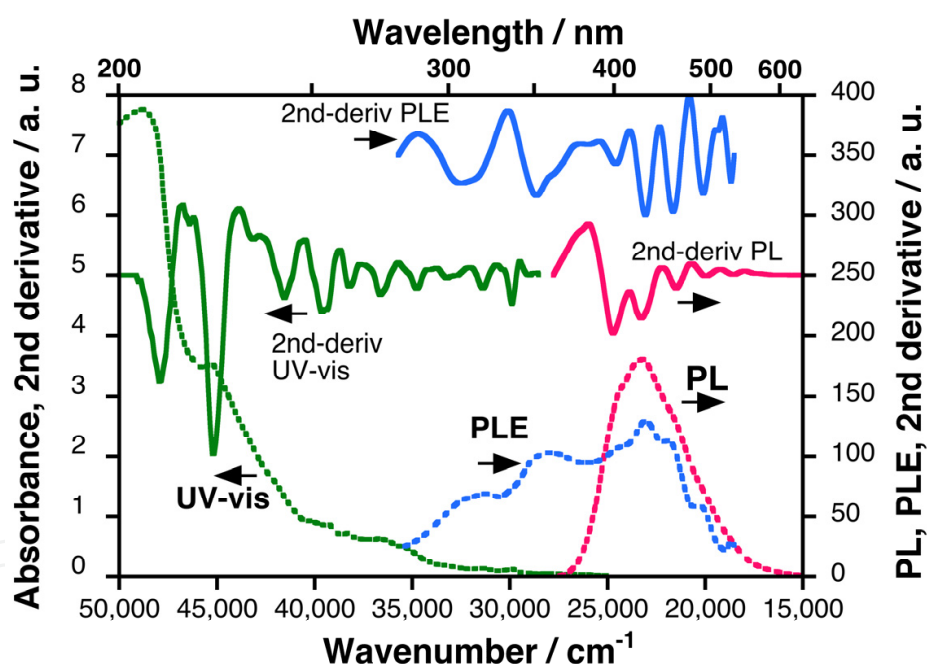


Fig. 9. PL excited at 360 nm, PL excitation (PLE) monitored at 540 nm, and UV-visible absorption spectra with their corresponding second derivative spectra for the air-exposed *nc*-like-Si particles dispersed in *n*-hexane.

Although exact  $\Phi_F$  values for these films were not determined, they were assumed to be several% (not exceeding 10%) at 77 K, and the PL intensities of the films at room temperature decreased by one-sixth compared to those at 77 K. This estimation was based on the fact that the  $\Phi_F$  value of virgin *n*-BSNP in THF solution at room temperature is ~1% using 9,10-diphenylanthracene as the reference ( $\Phi_F$  ~97% in methylcyclohexane). As for the *n*-BSNP film pyrolyzed at 300 °C, the PL band at 560 nm with excitation at 370 nm had fast

and slow lifetime components of  $\sim 5$  nsec and  $>10$  nsec, respectively, at 77 K. This short lifetime can be compared to the long lifetime of *c*-Si of 4.6 hrs (Lockwood, 1998; Yu and Cardona, 2005). An oxygen molecule may be inserted into the SNP skeleton because the SNP film was sealed in the presence of a small amount of air ( $\sim 3 \times 10^{-1}$  Torr). In fact, the film sealed in a trace amount of air ( $\sim 5 \times 10^{-5}$  Torr) exhibited a major PL band around 550 nm that was almost unchanged, even after thermal treatment at 200 and 300 °C. Controlling the time and temperature of the air-oxidation and pyrolysis of the virgin SNP film may thus facilitate fine tuning of the PL wavelength between 460 nm (2.70 eV) and 740 nm (1.66 eV).

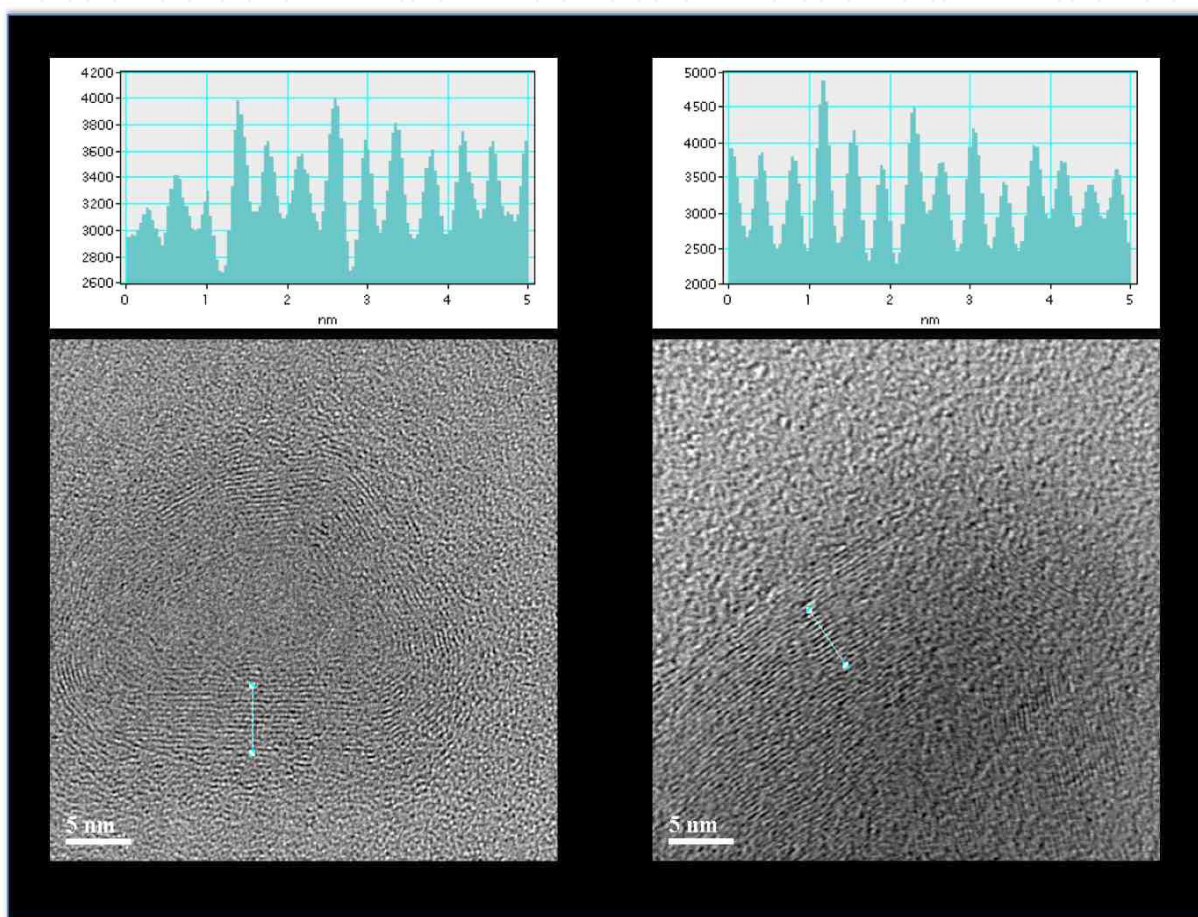


Fig. 10. HRTEM images of the air-exposed *nc*-Si particles. Left-side image: Baum-küchen-like, multi-layered structures with circular shapes and  $\sim 0.34$  nm spacing. Right-side image: Baum-küchen-like, lamellar shapes with  $\sim 0.37$  nm spacing. Surface profile at indicated location. Scale bar is 5 nm.

When the very weakly emitting Si particles in deep-red, which were produced by the pyrolysis of *n*-BSNP at 500 °C for 90 min, were exposed to air, the PL switched abruptly to an intense sky-blue color ( $\lambda = 430$  nm). The air-exposed Si particles, dispersed in common organic solvents at room temperature, exhibited an extremely high  $\Phi_F$  of 20–25% and a short lifetime of  $\sim 5$  nsec, probably due to the presence of siloxene-like, multi-layered Si-sheet structures.

$$E_n = \hbar^2 / 2m \cdot (\pi / na)^2, \text{ purely electronic transitions with } n \quad (1)$$



$$E_n = (n + 1/2) \hbar \omega, \square \text{ purely vibronic transitions with } n \quad (2)$$

The PL (excited at 360 nm), PL excitation (PLE, monitored at 540 nm), and UV-visible absorption spectra of the air-exposed Si particles dispersed in *n*-hexane are shown with the corresponding second derivative spectra in Fig. 9. Based on the second derivative spectra, the apparent broad PL, PLE, and absorption spectra consist of at least five well-resolved bands with almost equal energy spacing ( $1650 \pm 100 \text{ cm}^{-1}$  for the UV-visible absorption spectra,  $1580 \pm 200 \text{ cm}^{-1}$  for the PL spectra,  $1470 \pm 70 \text{ cm}^{-1}$  for the PLE spectra).

This periodic behavior may be related to the combination of bands arising from the Si-Si stretching mode ( $\sim 460 \text{ cm}^{-1}$ ) of the 2D-like Si skeleton and the Si-O-Si stretching mode ( $\sim 1100 \text{ cm}^{-1}$ ). Specifically, a coupling between an electron (from the Si-Si skeleton) and a phonon (from the Si-O-Si stretching vibration) is responsible for the strongly blue emission, due to the loss of translational symmetry. If the multiple electronic transitions in the PL, PLE, and UV-visible spectra came from purely electronic origins within the 2D structure, the energy separation ( $E_n$ ) should obey the inverse square of the quantum number,  $n$  (Eq. 1). If the transitions were connected to vibronic transitions, the separation would be related to  $n$  in a parabolic potential well (Eq. 2). The unexposed *nc*-like-Si samples may be of the former type due to very weak electron-phonon coupling, whereas the air-exposed *nc*-like-Si particles are presumably an example of the latter case [Yu and Cardona, 2005; Konagai, 1987; Davies, 1998, Colvin et al., 1994].

### 2.3 Structural analysis of the pyrolytic products by high-resolution transmission electron microscopy and laser Raman spectroscopy

The blue- and red-emissive structures of the air-exposed Si particles in the pyrolysis products were investigated by high-resolution transmission electron microscopy (HRTEM) with EDS. The HRTEM images of the air-exposed Si particles are shown in Fig. 10. The majority of the image regions show finely featured *nc*-Si particles with a diameter of  $\sim 1 \text{ nm}$  and a lattice spacing of  $\sim 2.5 \text{ \AA}$ . EDS analysis revealed the existence of oxygen in the image regions with a Si/O ratio of  $\sim 1/3$ . It is interesting that the two HRTEM images clearly show 'Baum-küchen-like' multi-layered structures; the left-side image in Fig. 10 shows circular shapes with  $\sim 3.4 \text{ \AA}$  spacing while the right-side image in Fig. 10 shows lamellar shapes with  $\sim 3.7 \text{ \AA}$  spacing. The *n*-BSNP exhibited a *d*-spacing of  $5.5 \text{ nm}$  ( $2\theta \sim 16^\circ$ ,  $\text{CuK}\alpha$ ) in a WAXD pattern, indicating that an interlayer spacing was present between *n*-BSNP multi-sheets, whereas the pyrolyzed *n*-BSNP does not show any ordered structures. These layered structures imply that the air-exposed Si particles have a 2D-Wöhler-siloxene structure (Brandt et al., 2003, Nesper, 2003) separated by a highly stretched Si-O-Si bond with an opened Si-O-Si bond angle, which is regarded to be a chemically well-controlled Zintl phase. The origin of the blue-shifted PL band at  $250^\circ \text{C}$  is assumed to be due to the partial oxidation of the SNP single-sheet when oxygen gas in the sealed tube is consumed during pyrolysis.

In nearly oxygen-free sealed conditions, a blue-shifted PL was not observed when the SNPs were treated at  $200\text{--}300^\circ \text{C}$ . The origin of the progressively red-shifted PL band at more elevated temperatures can be conjectured to be multi-layered with the spontaneous, stacked structure of 2D-SNP single-sheets, formed through the elimination of the organic moieties and hydrogen during pyrolysis. The PL wavelength is variable according to the thickness of the Si film (Lu et al., 1995). When an Si-Si bond length projected in the stacking direction is assumed to be  $1.85 \text{ \AA}$ , the Si layer number extrapolated from the PL peak wavelength can be



calculated using  $E_{\text{PL}} \text{ (eV)} = 1.6 + 0.7/d_{\text{Si}}^2$ , which is given for the Si/SiO<sub>2</sub> superlattice (Lu et al., 1995).

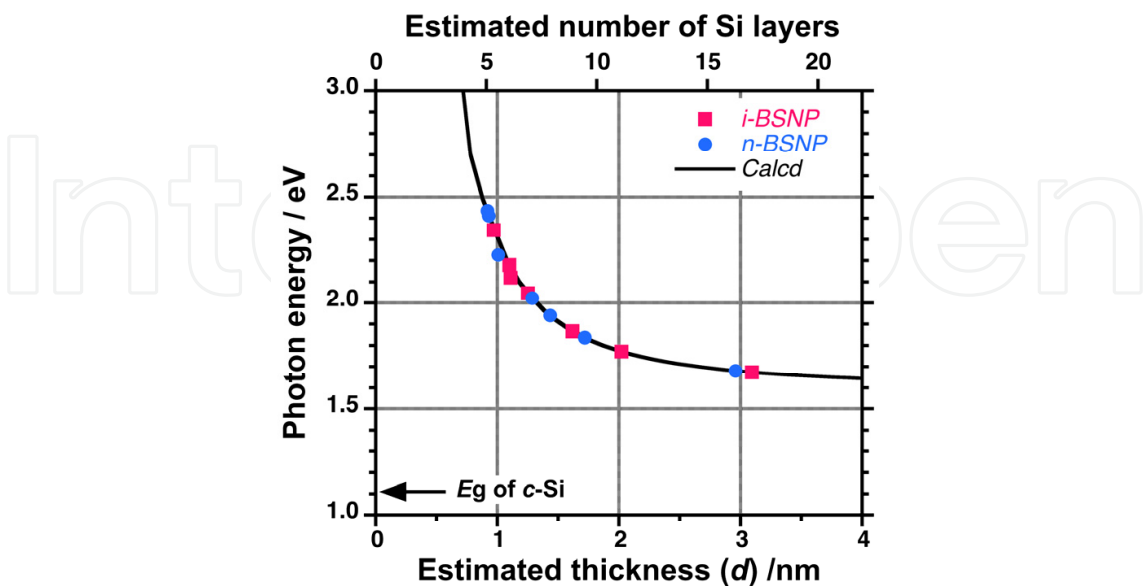


Fig. 11. Estimated numbers of Si multi-layers extrapolated from the PL peak energy of *n*-BSNP and *i*-BSNP, based on the equation ( $E_{\text{PL}}(\text{eV}) = 1.6 + 0.7/d_{\text{Si}}^2$ ) for the Si/SiO<sub>2</sub> superlattice (Lu et al., 1995).

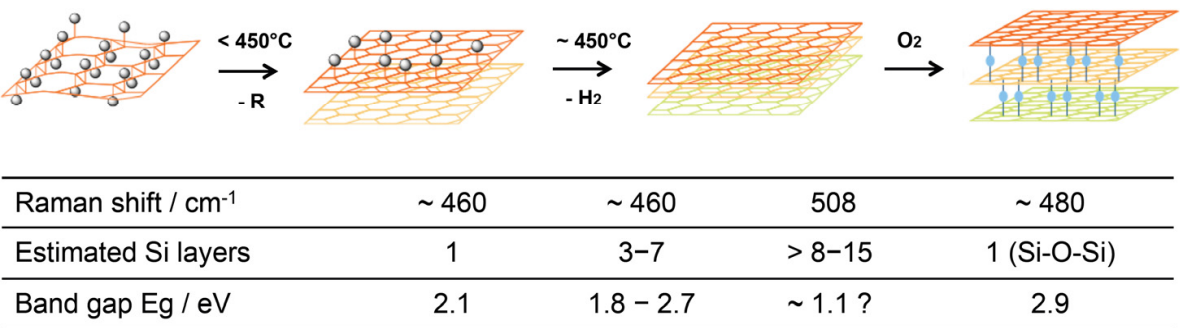


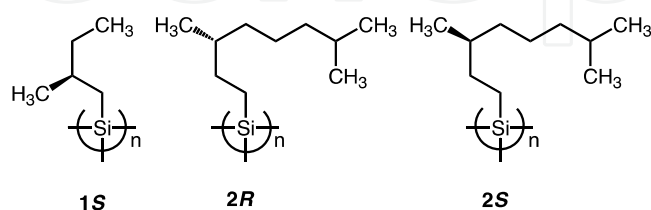
Fig. 12. Proposed scheme for changes in the structural hierarchy of SNP from 2D single-sheet to quasi-3D multi-sheets based on a Wöhler-siloxene-like structure with and without Si-O-Si interlayer spacers.

The PL energy in eV is plotted as a function of estimated thickness and number of Si layers in Fig. 11. When the pyrolyzed SNP without organic or H moieties was exposed to air, the spontaneous insertion of oxygen atoms into the multi-layer Si ultrathin films occurred, resulting in the formation of a periodic (Si)<sub>1</sub>/(SiO<sub>2</sub>)<sub>1</sub> superlattice (Lu et al., 1995) identical to the Wöhler-siloxene multi-layers (Brandt et al., 2003) with Si-O-Si interspacing. A previous study predicted that a Wöhler-siloxene structure bearing oxygen moieties would be highly emissive due to changes in electronic transitions from indirect- to direct-type band structures (Kanemitsu et al., 1993). This change results from characteristic  $\sigma$ -*n* orbital mixing of the 2D-Si  $\sigma$  electrons with the lone pair electrons of oxygen at the band-edge states for an ideal 2D-Si polymer bearing OH and H side groups (Takeda and Shiraishi, 1993).

Based on the results shown above, a change in hierarchical structure based on a model of Wöhler-siloxene multi-sheet layers separated by an Si-O-Si linkage at elevated pyrolysis temperatures, followed by exposure to air, is proposed in Fig. 12.

## 2.4 Circularly polarized light from chiral SNPs

The generation, amplification, and switching of circularly polarized luminescence (CPL) and circular dichroism (CD) by polymers (Chen et al., 1999; Oda et al., 2000; Kawagoe et al., 2010), small molecules (Lunkley et al., 2008; Harada et al., 2009), and solid surface crystals (Furumi and Sakka, 2006; Krause & Brett, 2008; Iba et al., 2011) have received considerable theoretical and experimental attention.



Scheme 5. Soluble, optically-active SNPs bearing chiral organic groups.

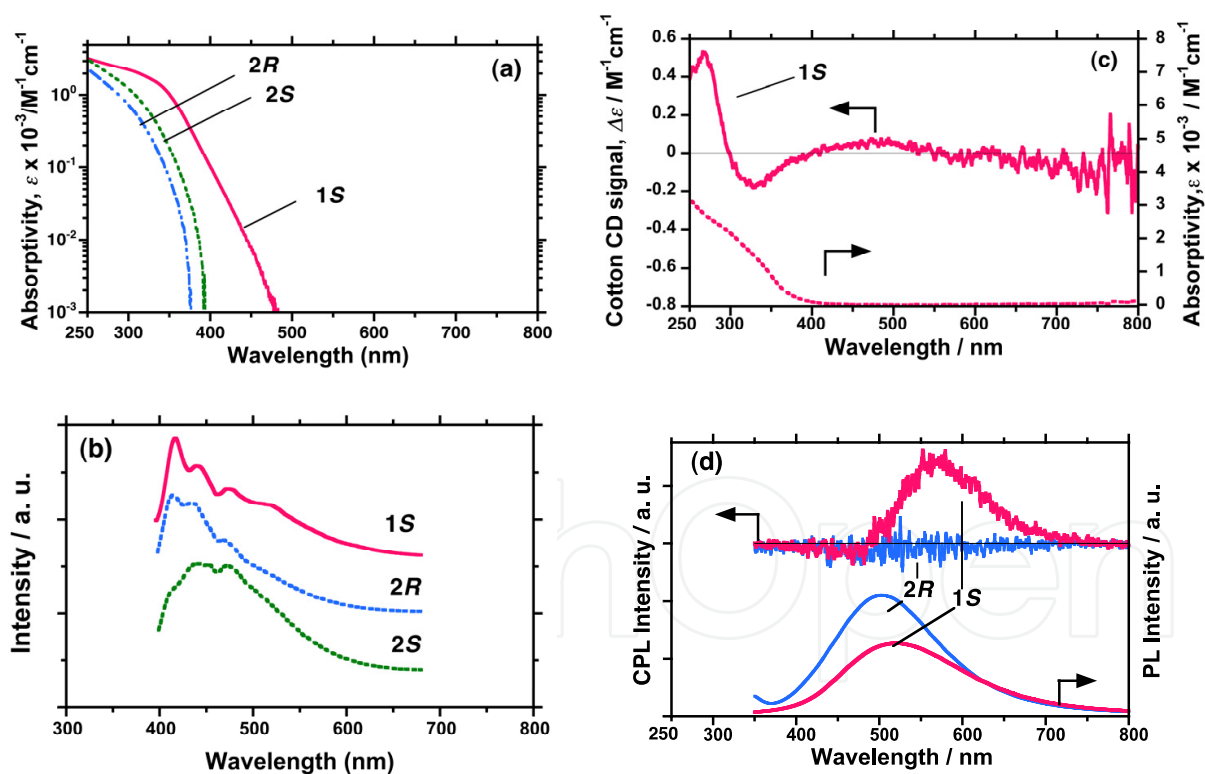


Fig. 13. UV-visible, PL, CD, and CPL spectra of **1S**, **2S**, and **2R** in THF at 25 °C.

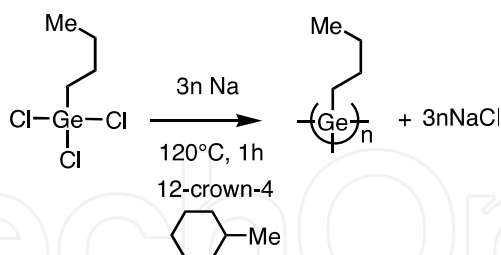
CPL is inherent to asymmetric luminophores in the excited state, whereas CD is due to asymmetric chromophores in the ground state. The first chiroptical (CPL and CD) properties of three new SNPs bearing chiral alkyl side groups (Fukao & Fujiki, 2009) were recently demonstrated for poly[(*S*)-2-methylbutylsilyl] (**1S**), poly[(*R*)-3,7-dimethyloctylsilyl] (**2R**), and poly[(*S*)-3,7-dimethyloctylsilyl] (**2S**) (Scheme 5).

This study revealed that only **1S**, bearing  $\beta$ -branched chiral groups, clearly showed an intense CPL signal at  $\sim 570$  nm with  $\Phi_F$  of  $\sim 1\%$  along with corresponding Cotton CD signals in THF solution at room temperature (Fig. 13). In contrast, **2R** and **2S**, which possess  $\gamma$ -branched chiral groups, did not exhibit any CPL signals although they did exhibit CD bands. By analogy to the optically inactive SNPs described above, optically active SNPs might be candidates for use as Si-source materials in the production of *a*-Si and *c*-Si films that exhibit circular polarization via controlled vacuum pyrolysis.

## 2.5 A Ge-Ge bonded network polymer (GNP) as an SNP analogue

Our understanding of the Si-Si bonded network polymeric materials led us to investigate a 2D Ge-Ge bonded network polymer (GNP) as a soluble model of insoluble polygermyne. A common approach for studying Si- and Ge-based materials is to effectively confine a photoexcited electron-hole pair within the Bohr radius ( $r_B$ ) for Si ( $r_B \sim 5$  nm) and for Ge ( $r_B \sim 24$  nm) (Gu et al., 2001). However, research on low-dimensional Ge-based materials has been delayed due to the limited synthetic approaches available for preparing soluble Ge-Ge bonded materials using organogermanium sources, which are 1000 times more expensive than the corresponding organosilane sources. Several Ge-based materials were recently fabricated using the molecular beam epitaxy (MBE) technique in an ultrahigh vacuum using inexpensive Ge-based inorganic sources, rapidly increasing their potential use in the fields of physics and applied physics.

In the area of solid-state physics, Kanemitsu, Masumoto, and coworkers observed a broad PL band at 570 nm (2.18 eV) for microcrystalline Ge ( $\mu$ c-Ge) embedded into SiO<sub>2</sub> glass at room temperature (Maeda et al., 1991). Stutzmann, Brandt, and coworkers reported a near infrared PL band at 920 nm (1.35 eV) for multi-layered Ge sheets produced on a solid surface, which is a pseudo-2D multi-layered Ge crystal known as polygermyne synthesized from Zintl-phase CaGe<sub>2</sub> (Vogg et al., 2000). However,  $\mu$ c-Ge, polygermyne, and polysiloxene are purely inorganic and are thus insoluble in any organic solvent.



Scheme 6. Synthesis of soluble *n*-butyl GNP.

In 1993, Bianconi et al. reported the first synthesis of GNP via reduction of *n*-hexyltrichlorogermane with a NaK alloy under ultrasonic irradiation (Hymanclki et al., 1993). However, the photophysical properties of GNP have not yet been reported in detail. In 1994, Kishida et al. reported that poly(*n*-hexylgermyne) at 77 K possesses a green PL band with a maximum at 560 nm (2.21 eV) whereas poly(*n*-hexylsilyne) exhibits a blue PL band around 480 nm (2.58 eV) (Kishida et al., 1994).

By applying our modified technique to a soluble GNP bearing *n*-butyl groups (*n*-BGNP) and through careful polymer synthesis (Scheme 6) and measurement of the PL, we briefly demonstrated that *n*-BGNP exhibits a very brilliant red PL band at 690 nm (1.80 eV). This result was obtained using a vacuum at 77 K without the pyrolysis process; under these

conditions, *n*-BSNP reveals a very brilliant green-colored PL band at 540 nm (2.30 eV) (Fig. 14) (Fujiki et al., 2009). This result differs from that of a previous report of green PL from poly(*n*-hexylgermyne) (Kishida et al., 1994).

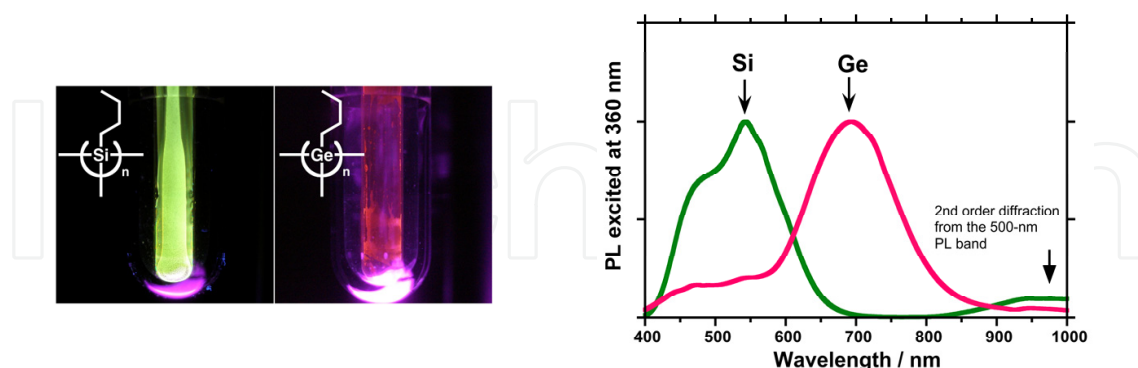


Fig. 14. Photographs (left) and PL spectra (right) of *n*-BSNP and *n*-BGNP films excited at 365 nm at 77 K.

By analogy with the SNPs described above, GNP may have potential uses as NIR emitters and narrow band gap materials with a loss of organic moieties by the pyrolysis process. In recent years, several studies have demonstrated the preparation and characterization of Ge nanoclusters capped with organic groups. Watanabe et al. elucidated that pyrolysis products of soluble Ge-Ge bonded nanoclusters capped with organic groups offer high-carrier mobility and optical waveguide with a high-refractive index value in semiconducting materials (Watanabe et al., 2005). Klimov et al. recently reported the presence of a near IR PL band at 1050 nm (1.18 eV) with a fairly high  $\Phi_F$  of 8% for *nc*-Ge capped with 1-octadecene, enabling a great reduction in Ge surface oxidation due to formation of strong Si-C bonds (Lee et al., 2009). The study of GNP pyrolysis is in progress and will be reported in the future.

## 2.6 Scope and perspectives

In recent years, solution processes for the fabrication of electronic and optoelectronic devices, as alternative methods to the conventional vacuum and vapor phase deposition processes, have received significant attention in a wide range of applications due to their many advantages, including processing simplicity, reduction in total production costs, and safety of chemical treatments. Particularly, the utilization of liquefied source material of an air-stable, non-toxic, non-flammable, non-explosive solid may be essential in some potential applications in printed semiconductor devices for large-area flexible displays, solar cells, and thin-film transistors (TFTs). Recent progress in this area has largely been focused on organic semiconductors with  $\pi$ -conjugated polymers due to their ease of processing, some of which have a relatively high carrier mobility that is comparable to that of *a*-Si.

Because of their ease of coating and dispersion in the form of 'Si-ink' in comparison to II-VI group nanocrystals [Colvin et al., 1994], soluble SNP, GNP, and their pyrolysis products can serve as Si-/Ge-source materials for the production of variable range Si-based and/or Si-Ge alloyed semiconductors at room temperature. The ionization potential of the pyrolyzed Si materials range between 5.2 and 5.4 eV while the electron affinity ranges between 4.0 and 3.2 eV (Lu et al., 1995). These values are well-matched with the work-functions of ITO and

Al/Ag/Mg electrodes. Recently, air stable red-green-blue emitting *nc*-Si was achieved using a SiH<sub>4</sub> plasma following CF<sub>4</sub> plasma etching (Pi et al., 2008). As an alternative method, laser ablation of bulk *c*-Si in supercritical CO<sub>2</sub> after excitation with a 532-nm nanosecond pulsed laser yielded *nc*-Si that could produce blue, green, and red emitters. (Saitow & Yamamura, 2009). As we have demonstrated, controlled vacuum pyrolysis using a single SNP source material, possibly including GNP source material, should offer a new, environmentally friendly, safer process to efficiently produce red-green-blue-near infrared emitters, thin films for TFTs, and solar cells because the required technology is largely compatible with XeCl excimer laser annealing and the crystallization process for making poly-Si TFTs from *a*-Si thin films deposited using the SiH<sub>4</sub>-Si<sub>2</sub>H<sub>6</sub> CVD process.

The dimensionality of inorganic materials makes it possible to tailor the band gap value, as shown in Table 1. Soluble SNP and GNP, because of their ease of coating and dispersion in the form of "Si-ink" and "Ge-ink", may serve as controlled soluble Si/Ge source materials without the need for the SiH<sub>4</sub>/GeH<sub>4</sub> CVD process. Our results provide a better understanding of the intrinsic nature of pseudo-2D Si electronic structure by varying Si layer numbers. The chemistry of SNP vacuum pyrolysis opens a new methodology to safely produce *a*-Si, *c*-Si, Si-based semiconductors, and alloys with Ge.

### 3. Summary

Although *c*-Si is the most archetypal semiconducting material for microelectronics, it is a poor visible emitter with a quantum yield of 0.01% at 300 K and a long PL lifetime of several hours. Pyrolysis of chain-like Si-containing polysilane and polycarbosilane has previously been shown to efficiently produce  $\beta$ -SiC; however, our TGA and ITGA pyrolysis experiments with various soluble SNPs indicated that elemental Si is produced. The SNP was transformed into a visible emitter that is tunable from 460 nm (2.7 eV) to 740 nm (1.68 eV) through control of the pyrolysis temperature and time (200–500 °C, 10–90 min). Moreover, air-exposed *nc*-like-Si, produced by pyrolyzing SNP at 500 °C, showed an intense blue PL with a maximum at 430 nm, a quantum yield of 20–25%, and a short lifetime of ~5 nsec; furthermore, these particles disperse in common organic solvents at room temperature. HRTEM, laser-Raman, and second-derivative UV-visible, PL, and PLE spectra indicated that the siloxene-like, multi-layered Si-sheet structures are responsible for the wide range of visible PL colors with high quantum yields. Circular polarization for SNPs bearing chiral side groups was also demonstrated for the first time. Through an analogous synthesis to that of green photoluminescent SNPs, the Ge-Ge bonded network polymer, GNP, was determined to be a red photoluminescent material.

### 4. Acknowledgements

This work was fully supported by the Nippon Sheet Glass Foundation for Materials Science and Engineering and partially supported by a Grant-in-Aid for Scientific Research (B) from MEXT (22350052, FY2010–FY2013). The authors thank Prof. Kyozauro Takeda, Prof. Kenji Shiraishi, Prof. Nobuo Matsumoto, Prof. Masaie Fujino, Prof. Akira Watanabe, Prof. Masanobu Naito, Prof. Kotohiro Nomura, Prof. Akiharu Satake, Dr. Kazuaki Furukawa, Dr. Anubhav Saxena, and our students, Dr. Masaaki Ishikawa, Satoshi Fukao, Dr. Takuma Kawabe, Yoshiki Kawamoto, Masahiko Kato, Yuji Fujimoto, Tomoki Saito, and Shin-ichi Hososhima for their helpful discussions and contributions.



## 5. References

- Alivisatos, A. P. (1996). Perspectives on the physical chemistry of semiconductor nanocrystals. *The Journal of Physical Chemistry*, Vol. 100, No. 31, 13226-13239.
- Bianconi, P. A.; Schilling, F. C. & Weidman, T. W. (1989). Ultrasound-mediated reductive condensation synthesis of silicon-silicon-bonded network polymers. *Macromolecules*, Vol. 22, No. 4, 1697-1704.
- Bianconi, P. A. & Weidman, T. W. (1988). Poly(*n*-hexylsilyne): Synthesis and properties of the first alkyl silicon [RSi]<sub>n</sub> network polymer. *Journal of the American Chemical Society*, 1988, Vol. 110, No. 7, 2342-2344.
- Brus, L. (1994). Luminescence of silicon materials: chains, sheets, nanocrystals, nanowires, microcrystals, and porous silicon. *The Journal of Physical Chemistry*, Vol. 98, No. 14, 3575-3581.
- Bley, R. A. & Kauzlarich, S. M. (1996). A low-temperature solution phase route for the synthesis of silicon nanoclusters. *Journal of the American Chemical Society*, Vol. 118, No. 49, 12461-12462.
- Brandt, M. S.; Vogg, G. & Stutzmann, M. (2003). *Silicon- and Germanium-Based Sheet Polymers and Zintl Phases*, in Jutzi, P. & Schubert, U. (eds.), *Silicon Chemistry*, ISBN-13: 978-3527306473, Wiley-VCH, Weinheim, Chapter 15, pp. 194-213.
- Chen, S. H., Katsis, D., Schmid, A. W., Mastrangelo, J. C., Tsutsui, T. & Blanton, T. N. (1999). Circularly polarized light generated by photoexcitation of luminophores in glassy liquid-crystal films. *Nature*, Vol. 397, 11 February 1999, 506-508.
- Choi, J.; Wang, N. S. & Reipa, V. (2007). Photoassisted tuning of silicon nanocrystal photoluminescence. *Langmuir*, Vol. 23, No. 6, 3388-3394.
- Colvin, V. L.; Schlamp, M. C. & Alivisatos, A. P. (1994). Light-emitting diodes made from cadmium selenide nanocrystals and a semiconducting polymer, *Nature*, Vol. 370, 4 August 1994, 354-357.
- Cullis, A. G. & Canham, L. T. (1991). Visible light emission due to quantum size effects in highly porous crystalline silicon. *Nature*, Vol. 353, 26 September 1991, 335-338.
- Cullis, A. G.; Canham, L. T. & Calcott, P. E. J. (1997). The structural and luminescence properties of porous silicon. *Journal of Applied Physics*, Vol. 82, No. 3, 909-965.
- Davies, J. H. (1998). *The Physics of Low-dimensional Semiconductors: An Introduction*, ISBN-13: 978-0521484916, Cambridge University Press, Cambridge.
- Diener, J.; Kovalev, D.; Koch, F. & Tsybeskov, L. Ordering and self-organization in nanocrystalline silicon. *Nature* 2000, Vol. 407, 21 September 2000, 358-361.
- English, D. S.; Pell, L. E.; Yu, Z.; Barbara, P. F. & Korgel, B. A. (2002). Size tunable visible luminescence from individual organic monolayer stabilized silicon nanocrystal quantum dots. *Nano Letters* Vol. 2, No. 7, 681-685.
- Fujiki, M. (2001). Optically active polysilylenes: State-of-the-art chiroptical polymers. *Macromolecular Rapid Communications*, Vol. 22, No. 8, 539-563.
- Fujiki, M.; Kawamoto, Y.; Kato, M.; Fujimoto, Y.; Saito, T.; Hososhima, S.-i. & Kwak, G. (2009). Full-visible-spectrum emitters from pyrolysis of soluble Si-Si bonded network polymers. *Chemistry of Materials*, Vol. 21, No. 12, 2459-2466.
- Fujiki, M.; Kato, M.; Kawamoto, Y. & Kwak, G. (2011). Green-and-red photoluminescence from Si-Si and Ge-Ge bonded network homopolymers and copolymers. *Polymer Chemistry*, Vol. 2, No. 4, 914-922.

- Fojtik, A. & Henglein, A. (1994). Luminescent colloidal silicon particles. *Chemical Physics Letters*, Vol. 221, No. 5–6, 363–367.
- Fukao, S. & Fujiki, M. (2009). Circularly polarized luminescence and circular dichroism from Si-Si-bonded network polymers. *Macromolecules*, Vol. 42, No. 21, 8062–8067.
- Furukawa, K.; Fujino, M. & Matsumoto, N. (1990). Optical properties of silicon network polymers. *Macromolecules*, Vol. 23, No. 14, 3423–3426.
- Furukawa, K. (2000). *Synthesis and Optical Properties of Silicon-backbone Materials: (RSi)<sub>n</sub>* (R = Organic group), Doctor thesis, Waseda University, Tokyo, Japan, Chapter 7 (in Japanese).
- Furukawa, S. & Miyasato, T. (1988). Quantum size effects on the optical band-gap of microcrystalline Si-H. *Physical Review B*, Vol. 38, No. 8, 5726–5729.
- Furumi, S. & Sakka, Y. (2006). Chiroptical properties induced in chiral photonic-bandgap liquid crystals leading to a highly efficient laser-feedback effect. *Advanced Materials*, Vol. 18, No. 6, 775–780.
- Gelloz, B.; Kojima, A. & Koshida, N. (2005). Highly efficient and stable luminescence of nanocrystalline porous silicon treated by high-pressure water vapor annealing. *Applied Physics Letters*, Vol. 87, No. 3, 031107.
- Gu, G.; Burghard, M.; Kim, G. T.; Düsberg, G. S.; Chiu, P. W.; Krstic, V.; Roth, S. & Han, W. Q. (2001). Growth and electrical transport of germanium nanowires. *Journal of Applied Physics*, 2001, Vol. 90, No. 11, 5747–5751.
- Harada, T., Nakano, Y., Fujiki, M., Naito, M., Kawai, T. & Hasegawa, Y. (2009). Circularly polarized luminescence of Eu(III) complexes with point- and axis-chiral ligands dependent on coordination structures. *Inorganic Chemistry*, Vol. 48, No. 23, 11242–11250.
- Hasegawa, T.; Iwasa, Y.; Koda, T.; Kishida, H.; Tokura, Y.; Wada, S.; Tashiro, H.; Tachibana, H. & Matsumoto, M. (1996). Nature of one-dimensional excitons in polysilanes. *Physical Review B*, Vol. 54, No. 16, 11365–11374.
- Heitmann, J.; Möller, F.; Zacharias, M. & Gösele, U. (2005). Silicon nanocrystals: size matters. *Advanced Materials*, Vol. 17, No. 7, 795–803.
- Holmes, J. D.; Ziegler, K. J.; Doty, R. C.; Pell, L. E.; Johnston, K. P. & Korgel, B. A. (2001). Highly luminescent silicon nanocrystals with discrete optical transitions. *Journal of the American Chemical Society*, Vol. 123, No. 16, 3743–3748.
- Hua, F.; Erogbogbo, F.; Swihart, M. T. & Ruckenstein, E. (2006). Organically capped silicon nanoparticles with blue photoluminescence prepared by hydrosilylation followed by oxidation. *Langmuir*, Vol. 22, No. 9, 4363–4370.
- Hymancski, W. J.; Vicscher, G. T. & Bianconi, P. A. (1993). Polygermynes: Synthesis and properties of germanium-germanium bonded network polymers. *Macromolecules*, 1993, Vol. 26, No. 4, 869–871.
- Iba, S., Koh, S., Ikeda, K. & Kawaguchi, H. (2011). Room temperature circularly polarized lasing in an optically spin injected vertical-cavity surface-emitting laser with (110) GaAs quantum wells. *Applied Physics Letters*, Vol. 98, No. 8, 081113 (2011).
- Jurbergs, D.; Rogojina, E.; Mangolini, L. & Kortshagen, U. (2006). Silicon nanocrystals with ensemble quantum yields exceeding 60%. *Applied Physics Letters*, Vol. 88, No. 23, 233116.

- Kanemitsu, Y.; Ogawa, T.; Shiraishi, K. & Takeda, K. (1993). Visible photoluminescence from oxide Si nanometer-sized spheres - Exciton confinement on a spherical-shell. *Physical Review B*, Vol. 48, No. 7, 4883–4886.
- Kanemitsu, Y. (1996). Photoluminescence spectrum and dynamics in oxidized silicon nanocrystals: A nanoscopic disorder system. *Physical Review B*, Vol. 53, No. 20, 13515–13520.
- Kawagoe, Y., Fujiki, M. & Nakano, Y. (2000). Limonene magic: noncovalent molecular chirality transfer leading to ambidextrous circularly polarised luminescent  $\pi$ -conjugated polymers. *New Journal of Chemistry*, Vol. 34, No. 4, 637–647.
- Kishida, H.; Tachibana, H.; Matsumoto, M. & Tokura, Y. (1994). Optical spectra of Si/Ge-network copolymers:  $[\text{Si}(\text{C}_6\text{H}_{13})]_{1-x}[\text{Ge}(\text{C}_6\text{H}_{13})]_x$ . *Applied Physics Letters*, 1994, Vol. 65, No. 11, 1358–1360.
- Kovalev, D.; Heckler, H.; Ben-Chorin, M.; Polisski, G.; Schwartzkopff, M. & Koch, F. (1998). Breakdown of the  $k$ -conservation rule in Si nanocrystals. *Physical Review Letters*, Vol. 81, No. 13, 2803–2806.
- Kovalev, D. & Fujii, M. (2005). Silicon nanocrystals: photosensitizers for oxygen molecules. *Advanced Materials*, Vol. 17, No. 21, 2531–2544.
- Konagai, M. (1987). *Handotai Chokoshi Nyumon (Introduction to Semiconductor Superlattice)*, ISBN-13: 978-4563034351, Baifukan, Tokyo (in Japanese).
- Krause, K. M. & Brett, M. J. (2008). Spatially graded nanostructured chiral films as tunable circular polarizers. *Advanced Functional Materials*, Vol. 18, No. 20, 3111–3118.
- Lee, D. C.; Pietryga, J. M.; Robel, I.; Werder, D. J.; Schaller, R. D. & Klimov, V. I. (2009). Colloidal synthesis of infrared-emitting germanium nanocrystals. *Journal of the American Chemical Society*, Vol. 131, No. 10, 3436–3437.
- Lehmann, V. & Gösele, U. (1991). The structural and luminescence properties of porous silicon. *Applied Physics Letters*, Vol. 58, No. 8, 856–858.
- Li, X.; He, Y. & Swihart, M. T. (2004). Surface functionalization of silicon nanoparticles produced by laser-driven pyrolysis of silane followed by HF-HNO<sub>3</sub> etching. *Langmuir*, Vol. 20, No. 11, 4720–4727.
- Liu, Q.; Wu, H.-J.; Lewis, R.; Maciel, G. E. & Interrante, L. V. (1999). Investigation of the pyrolytic conversion of poly(silylenemethylene) to silicon carbide. *Chemistry of Materials*, Vol. 11, No. 8, 2038–2048.
- Liu, S.-M. (2008). Luminescent silicon nanoparticles formed in solution. *Journal of Nanoscience and Nanotechnology*, Vol. 8, No. 3, 1110–1125.
- Liu, S.-M.; Sato, S. & Kimura, K. (2005). Synthesis of luminescent silicon nanopowders redispersible to various solvents. *Langmuir*, Vol. 21, No. 14, 6324–6329.
- Liu, S.-M.; Yang, Y.; Sato, S. & Kimura, K. (2006). Enhanced photoluminescence from Si nano-organosols by functionalization with alkenes and their size evolution. *Chemistry of Materials*, Vol. 18, No. 3, 637–642.
- Lockwood, D. J. (1998). *Light Emission in Silicon*, in Lockwood, D. J. (ed.), *Light Emission in Silicon From Physics to Devices*, Academic Press, ISBN-13: 978-0127521572, New York, 1998. Chapter 1, pp 1–34.
- Lu, Z. H.; Lockwood, D. J. & Baribeau, J.-M. (1995). Quantum confinement and light emission in SiO<sub>2</sub>/Si superlattices. *Nature*, Vol. 378, 16 November 1995, 258–260.
- Lunkley, J. L., Shirotani, D., Yamanari, K., Kaizaki, S. & Muller, G. (2008). Extraordinary circularly polarized luminescence activity exhibited by cesium tetrakis(3-

- heptafluoro-butylryl-(+)-camphorato) Eu(III) complexes in EtOH and CHCl<sub>3</sub> Solutions. *Journal of the American Chemical Society*, Vol. 130, No. 42, 13814–13815.
- Maeda, Y.; Tsukamoto, N.; Yazawa, Y.; Kanemitsu, Y. & Masumoto, Y. (1991). Visible photoluminescence of Ge microcrystals embedded in SiO<sub>2</sub> glassy matrices. *Applied Physics Letters*, 1991, Vol 59, No. 24, 3168–3170.
- Ma, D. D. D.; Lea, S. T. & Shinar, J. (2005). Strong polarization-dependent photoluminescence from silicon nanowire fibers. *Applied Physics Letters*, Vol. 87, No. 3, 033107.
- Martin, H.-P.; Müller, E.; Richter, R.; Roewer, G. & Brendler, E. (1997). Methylchlorooligosilanes as products of the basecatalysed disproportionation of various methylchlorodisilanes. *Journal of Organometallic Chemistry*, Vol. 32, No. 1381–1387.
- Mayeri, D.; Phillips, B. L.; Augustine, M. P. & Kauzlarich, S. M. (2001). NMR study of the synthesis of alkyl-terminated silicon nanoparticles from the reaction of SiCl<sub>4</sub> with the Zintl salt, NaSi. *Chemistry of Materials*. Vol. 13, No. 3, 765–770.
- Nayfeh, M. & Mitas, L. (2008). *Silicon Nanoparticles: New Photonic and Electronic Material at the Transition Between Solid and Molecules*, in Kumar, V. (ed.), *Nanosilicon*, Elsevier, Oxford, ISBN-13: 978-0080445281, Chapter 1, pp. 1–78.
- Nesper, R. (2003). *Structural and Electronic Systematics in Zintl Phases of the Tetrrels*, in Jutzi, P. & Schubert, U. (eds.), *Silicon Chemistry*, ISBN-13: 978-3527306473, Wiley-VCH, Weinheim, Chapter 13, pp. 171–180.
- Oda, M.; Nothofer, H.G.; Lieser, G.; Scherf, U.; Meskers, S. C. & Neher, D. (2000). Circularly polarized electroluminescence from liquid-crystalline chiral polyfluorenes. *Advanced Materials*, Vol. 12, No. 5, 362–365.
- Pi, X. D.; Liptak, R. W.; Nowak, J. D.; Wells, N. P.; Carter, C. B.; Campbell, S. A. & Kortshage, U. (2008). Air-stable full-visible-spectrum emission from silicon nanocrystals synthesized by an all-gas-phase plasma approach. *Nanotechnology*, Vol. 19, No. 24, 245603.
- Qi, J.; Belcher, A. M. & White, J. M. (2003). Spectroscopy of individual silicon nanowires. *Applied Physics Letters*, Vol. 82, No. 16, 2616–2618.
- Saitow, K. & Yamamura, T. (2009). Effective cooling generates efficient emission: Blue, green, and red light-emitting Si nanocrystals. *The Journal of Physical Chemistry C*, Vol. 113, No. 19, 8465–8470.
- Schmidt, W. R.; Interrante, L. V.; Doremus, R. H.; Trout, T. K.; Marchetti, P. S. & Maciels, G. E. (1991). Pyrolysis chemistry of an organometallic precursor to silicon carbide. *Chemistry of Materials*, Vol. 3, No. 2, 257–267.
- Shimoda, T.; Matsuki, Y.; Furusawa, M.; Aoki, T.; Yudasaka, I.; Tanaka, H.; Iwasawa, H.; Wang, D.; Miyasaka, M. & Takeuchi, Y. Solution-processed silicon films and transistors. *Nature* 2006, Vol. 440, 6 April 2006, 783–786.
- Shini, K. & Kumada, M. (1958). Thermal rearrangement of hexamethyldisilane to trimethyl-(dimethylsilylmethyl)silane. *The Journal of Organic Chemistry*, Vol. 23, No. 1, 139–139.
- Smith, D. A.; Joray, S. J. & Bianconi, P. A. (2005). Synthetic method development and molecular weight control for homo- and co-polysilynes, silicon-based network-backbone polymers. *Journal of Polymer Research*, 2005, Vol. 12, No. 5, 393–401.
- Takagi, H.; Ogawa, H.; Yamazaki, A.; Ishizaki, A. & Nakagiri, T. (1990). Quantum size effects on photoluminescence in ultrafine Si particles. *Applied Physics Letters*, Vol. 56, No. 24, 2379–2381.



- Takeda, K.; Teramae, H. & Matsumoto, N. (1986). Electronic structure of chainlike polysilane. *Journal of the American Chemical Society*, Vol. 108, No. 26, 8186–8190.
- Takeda, K. & Shiraishi, K. (1989). Electronic structure of Si-skeleton materials. *Physical Review B*, Vol. 39, No. 15, 11028–11037.
- Takeda, K. & Shiraishi, K. (1993). Electronic structure of silicon-oxygen high polymers. *Solid State Communications*, Vol. 85, No. 4, 301–305.
- Teramae, H. & Takeda, K. (1989). Ab initio studies on silicon compounds. Part II. The gauche structure of the parent polysilane. *Journal of the American Chemical Society*, Vol. 111, No. 4, 1281–1285.
- Vogg, G.; Brandt, M. S. & Stutzmann, M. (2000). Polygermyne—A prototype system for layered germanium polymers. *Advanced Materials*, 2000, Vol. 12, No. 17, 1278–1281.
- Walters, R. J.; Kalkman, J.; Polman, A.; Atwater, H. A. & de Dood, M. J. A. (2006). Photoluminescence quantum efficiency of dense silicon nanocrystal ensembles in SiO<sub>2</sub>. *Physical Review B*, Vol. 73, No. 13, 132302.
- Watanabe, A. (2003). Optical properties of polysilanes with various silicon skeletons. *Journal of Organometallic Chemistry*, Vol. 685, No. 1-2, 122–133.
- Watanabe, A.; Hojo, F. & Miwa, T. (2005). Field-effect transistor based on organosoluble germanium nanoclusters. *Applied Organometallic Chemistry*, Vol. 19, No. 4, 530–537.
- Wilcoxon, J. P.; Samara, G. A. & Provencio, P. N. (1999). Optical and electronic properties of Si nanoclusters synthesized in inverse micelles. *Physical Review B*, Vol. 60, No. 4, 2704–2714.
- Wilson, W. L. & Weidman, T. W. (1991). Excited-state dynamics of one- and two-dimensional  $\sigma$ -conjugated silicon frame polymers: dramatic effects of branching in a series of hexylsilyne-branched poly(hexylmethylsilylene) copolymers. *The Journal of Physical Chemistry*, Vol. 95, No. 11, 4568–4572.
- Wilson, W. L.; Szajowski, P. F. & Brus, L. E. (1993). Quantum confinement in size-selected, surface-oxidized silicon nanocrystals. *Science*, Vol. 262, No. 5137, 1242–1244.
- Yu, P. Y. & Cardona, M. (2005). *Fundamentals of Semiconductors: Physics and Materials Properties; 3rd Ed.*, Springer-Verlag, ISBN-13: 978-3540254706, Chapter 7, 345–426.
- Yajima, S.; Hasegawa, Y.; Hayashi, J. & Imura, M. (1978). Synthesis of continuous silicon carbide fibre with high tensile strength and high Young's modulus: Part 1. Synthesis of polycarbosilane as precursor. *Journal of Material Science*, Vol. 13, No. 12, 2569–2576.
- Zou, J.; Baldwin, R. K.; Pettigrew, K. A. & Kauzlarich, S. M. (2004). Solution synthesis of ultrastable luminescent siloxane-coated silicon nanoparticles. *Nano Letters*, Vol. 4, No. 7, 1181–1186.
- Zhang, X.; Brynda, M.; Britt, R. D.; Carroll, E. C.; Larsen, D. S.; Louie, A. Y. & Kauzlarich, S. M. (2007). Synthesis and characterization of manganese-doped silicon nanoparticles: Bifunctional paramagnetic-optical nanomaterial. *Journal of the American Chemical Society*, Vol. 129, No. 35, 10668–10669.



© 2011 The Author(s). Licensee IntechOpen. This chapter is distributed under the terms of the [Creative Commons Attribution-NonCommercial-ShareAlike-3.0 License](https://creativecommons.org/licenses/by-nc-sa/3.0/), which permits use, distribution and reproduction for non-commercial purposes, provided the original is properly cited and derivative works building on this content are distributed under the same license.

IntechOpen

IntechOpen